arXiv:0708.1910v2 [cond-mat.other] 13 Nov 2007

# Correlated behavior of conductance and phase rigidity in the transition from the weak-coupling to the strong-coupling regime

E.N. Bulgakov[1,2], I. Rotter[1] and A. F. Sadreev[1,2]

[1] *Max Planck Institute for the Physics of Complex Systems, D-01187 Dresden, Germany and*

[2] *Kirensky Institute of Physics, 660036, Krasnoyarsk, Russia*

(Dated: February 8, 2022)

## Abstract

We study the transmission through different small systems as a function of the coupling strength $v$ to the two attached leads. The leads are identical with only one propagating mode $\xi_C^E$ in each of them. Besides the conductance $G$, we calculate the phase rigidity $\rho$ of the scattering wave function $\Psi_C^E$ in the interior of the system. Most interesting results are obtained in the regime of strongly overlapping resonance states where the crossover from staying to traveling modes takes place. The crossover is characterized by collective effects. Here, the conductance is plateau-like enhanced in some energy regions of finite length while corridors with zero transmission (total reflection) appear in other energy regions. This transmission picture depends only weakly on the spectrum of the closed system. It is caused by the alignment of some resonance states of the system with the propagating modes $\xi_C^E$ in the leads. The alignment of resonance states takes place stepwise by resonance trapping, i.e. it is accompanied by the decoupling of other resonance states from the continuum of propagating modes. This process is quantitatively described by the phase rigidity $\rho$ of the scattering wave function. Averaged over energy in the considered energy window, $\langle G\rangle$ is correlated with $1-\langle\rho\rangle$. In the regime of strong coupling, only two short-lived resonance states survive each aligned with one of the channel wave functions $\xi_C^E$. They may be identified with traveling modes through the system. The remaining $M-2$ trapped narrow resonance states are well separated from one another.

## I. INTRODUCTION

Resonance phenomena in quantum systems at very low and at very high level density are well understood. In the first case, isolated resonances can be seen in the cross section whose decay widths are smaller than the distance between them. They are described well by means of the discrete states of the closed system. In the second case narrow resonances appear, superposed on a smooth background. Here, the resonance states are usually described on the basis of statistical assumptions while the background is represented by the so-called optical $S$ matrix [1]. Much less understood is the transition between these two borderline cases. In this crossover regime, the resonances overlap, and a full (standard) statistical description is, generally, not justified. For the results of numerical studies for a realistic system see, e.g., Ref. [2]. Characteristic features of the scenario with overlapping resonances are the avoided crossings of the resonance states in the complex plane which may change considerably the spectroscopic properties (such as positions and widths) of the states [3]. In order to describe these changes under realistic conditions (especially in the few-channel case), both the real *and* imaginary parts of the coupling via the continuum have to be taken into account. In the standard statistical approach, only the real part is considered. In the recent paper [4], only the imaginary part of the coupling via the continuum is taken into account. Here, serious deviations from the standard statistical approach are found. Strong deviations are found also when both the real and imaginary parts are considered [2]. Generally, the phases of the wave functions are not rigid in the regime of overlapping resonances as shown analytically in Ref. [5].

Mathematically, an open quantum system can be described best by a non-hermitian Hamilton operator that accounts not only for the energies but also for the widths (lifetimes) of the resonance states. Spectroscopic studies on the basis of a realistic non-hermitian Hamilton operator (with complex coupling term) are performed up to now either by using the method of complex scaling [6] or the method of the Feshbach projection operator technique [3]. The last method is applied also to the transmission through small devices. The theory for this case, presented in Ref. [7], is equivalent to the tight-binding lattice model [8]. In the numerical results, long-range correlations between the individual resonance states have been observed.

Most theoretical studies with non-hermitian Hamilton operators are based on random

matrices. Usually, the Pandey-Mehta Hamilton operator $H(\alpha) = H_0 + \alpha H_1$ is used where $H_0$ and $H_1$ are real and complex random hermitian matrices, respectively, and $\alpha$ is a crossover parameter [9]. Recent theoretical studies have shown that long-range correlations in the eigenfunctions of $H(\alpha)$ appear also in these studies [10]. The theoretical results are in good agreement with experimental ones obtained in an open microwave billiard [11].

In order to describe the intensity fluctuations generated by a monochromatic source in a disordered cavity coupled to the environment, the idea of *standing* waves in almost closed systems and *traveling* waves in open systems is considered in Ref. [12]. In this paper, the two borderline cases are related to one another by an interpolation procedure.

Another characteristic feature of overlapping resonances is the fluctuation picture of the cross section. The autocorrelation function shows Ericson fluctuations [13] studied experimentally first in nuclear reaction cross sections [14]. Recently they are studied experimentally with high resolution in the photoionization of rubidium atoms in crossed magnetic and electric fields [15]. The experimental results obtained in this study proved not only the universality of the Ericson fluctuations. They showed an unexpected high reproducibility of the results. This experimental result does not coincide with the usual understanding of the nature of Ericson fluctuations.

In recent theoretical studies on Ericson fluctuations, the importance of interferences between different resonance states is discussed. In Ref. [16] it is presumed that Ericson fluctuations do not result from interferences, but may be considered as a collective coherent resonance phenomenon. In the literature, this collective phenomenon is called resonance trapping. It is studied theoretically as well as experimentally [17] in many papers, see the reviews [3]. It is a collective effect caused by the decoupling of most of the resonance states from the continuum at large coupling strength between system and environment while only a few states become short-lived. This interpretation of Ericson fluctuations is called misinterpretation in Ref. [18] due to the result obtained by the author, that the fluctuations originate from interferences between random-partial-width amplitudes in the regime of strongly overlapping resonances.

It is the aim of the present paper to study the transmission through microwave cavities as well as through toy-model systems with a small number of sites (corresponding to a small number of levels) in the two-channel case (one in each of the attached leads) without using any statistical assumptions. The mathematical basis of our study is the Feshbach

projection operator [1] formalism, i.e. the non-hermitian effective Hamilton operator $H_{\rm eff}$ (see Sect. II) and its relation to the Green function $G_{\rm eff} = (E - H_{\rm eff})^{-1}$. The numerical results for microwave cavities (Sect. III) as well as for one-dimensional and two-dimensional toy-model systems with different positions of the attached wires (Sect IV) are obtained by using the tight-binding lattice Green function method [8] providing accurate results for sufficiently large numerical grids. We turn our attention especially to the appearance of coherent collective effects and long-range correlations in the crossover regime from standing to traveling waves, i.e. in the regime of overlapping resonances. Furthermore (Sect. V), we show the appearance of Ericson-like fluctuations. We are interested in the structure of the autocorrelation function for different values of the displacement and for different degrees of resonance overlapping. We comment also on the reproducibility of the results by changing the geometry of the system. The results are discussed and summarized in the last section.

## II. SPECTROSCOPIC VALUES OF AN OPEN QUANTUM BILLIARD

### A. Non-hermitian Hamilton operator of the open system

In an exact description of resonance phenomena by using the Feshbach projection operator technique [1], the non-hermitian effective Hamilton operator

$$H_{\rm eff} = H_B + \sum_{C=L,R} V_{BC} \frac{1}{E^+ - H_C} V_{CB} \tag{1}$$

appears where $H_B$ is the hermitian Hamilton operator of the corresponding closed system with $M$ discrete states, $V_{BC}$ is the symmetrical coupling operator between system and environment, $H_C$ is the hermitian Hamilton operator describing the propagating modes in the environment and $C$ stands for the continuum of propagating modes. In the case of a quantum cavity, $C$ consists of the waves in the right ($R$) and left ($L$) leads attached to the cavity [7]. In this representation, the resonance picture is determined by the eigenvalues $z_\lambda$ and eigenfunctions $\phi_\lambda$ of $H_{\rm eff}$, Eq. (1), which differ, generally, from those of $H_B$ not only by $\mathrm{Im}(z_\lambda) \neq 0$. Also $\mathrm{Re}(z_\lambda)$ differs from the (real) eigenvalue of $H_B$ by the contribution arising from the principal value integral of the second term of $H_{\rm eff}$.

The $M$ eigenvalues $z_\lambda$ of $H_{\rm eff}$ are complex and energy dependent. They provide the positions $E_\lambda$ and widths $\Gamma_\lambda$ of the resonance states by solving the fixed-point equations

$E_\lambda = \mathrm{Re}(z_\lambda)|_{E=E_\lambda}$ and defining $\Gamma_\lambda = -2\,\mathrm{Im}(z_\lambda)|_{E=E_\lambda}$. These values correspond to the poles of the $S$ matrix. However, for the $S$ matrix describing a physical scattering process at the real energy $E$ of the system (without any poles), the solutions of the fixed-point equations are relevant only for narrow resonances. Generally, the eigenvalues $z_\lambda$ with their full energy dependence are involved in the $S$ matrix [3].

Also the eigenfunctions $\phi_\lambda$ of $H_{\mathrm{eff}}$ are complex and energy dependent. The $\phi_\lambda$ are biorthogonal. Due to the symmetry of $H_{\mathrm{eff}}$, it holds [3],

$$\langle \phi_\lambda^* | \phi_{\lambda'} \rangle = \delta_{\lambda,\lambda'} \; . \tag{2}$$

As a consequence, $\langle \phi_\lambda | \phi_\lambda \rangle = A_\lambda \geq 1$ and $A_\lambda \to \infty$ with approaching the branch point at which two eigenvalues coalesce, $z_\lambda = z_{\lambda'}$ [19, 20, 21].

Considering the coupling strength $v$ as control parameter, the phenomenon of resonance trapping [3, 22] appears, i.e. the wave functions of a few resonance states align each with one of the channel wave functions while the other resonance states decouple from the continuum (become trapped). The resonance trapping occurs hierarchically [23, 24]. Some years ago, the phenomenon of resonance trapping is studied theoretically [25] and even proven experimentally [17] on microwave cavities.

The eigenfunctions $\phi_\lambda$ of $H_{\mathrm{eff}}$ can be represented in the set $\{\phi_\lambda^B\}$ of eigenfunctions of the Hamilton operator $H_B$ of the corresponding closed system,

$$\phi_\lambda = \sum_{\lambda'}^{M} d_{\lambda\lambda'} \; \phi_{\lambda'}^B \tag{3}$$

with complex coefficients $d_{\lambda\lambda'}$ normalized according to $|d_{\lambda\lambda'}|^2 / \sum_{\lambda''=1}^{M} |d_{\lambda'\lambda''}|^2$.

### B. Scattering wave function and transmission

The eigenfunctions $\phi_\lambda$ of $H_{\mathrm{eff}}$ are part of the total scattering wave function $\Psi_C^E$ that is solution of the Schrödinger equation $(H-E)\Psi_C^E = 0$ in the total function space consisting of the discrete states at the energies $E_\lambda^B$ of the closed quantum billiard and of the propagating modes $\xi_C^E$ in the attached leads. Due to the coupling between the two subspaces, the discrete states turn over into resonance states at the energies $E_\lambda$ of the open billiard. $H$ is hermitian. The $\Psi_C^E$ read [3]

$$\Psi_C^E = \xi_C^E + \sum_\lambda \Omega_\lambda^C \, \frac{\langle \phi_\lambda^* | V | \xi_C^E \rangle}{E - z_\lambda} \tag{4}$$

where $\Omega_\lambda^C = [1 + (E^+ - H_C)^{-1}V]\,\phi_\lambda$ is the wave function of the resonance state $\lambda$. According to (4), the eigenfunctions $\phi_\lambda$ of the effective Hamilton operator $H_{\rm eff}$ give an essential contribution to the scattering wave function $\Psi_C^E$ in the interior of the cavity, $\Psi_C^E \to \hat{\Psi}_C^E$, with

$$\hat{\Psi}_C^E = \sum_\lambda c_{\lambda E}\,\phi_\lambda\,; \qquad c_{\lambda E} = \frac{\langle \phi_\lambda^* | V | \xi_C^E \rangle}{E - z_\lambda}\,. \tag{5}$$

The coupling coefficients $\langle \phi_\lambda^* | V | \xi_C^E \rangle$ are, generally, complex and energy dependent due to the unitarity of the $S$ matrix [27]. This energy dependence becomes important only for overlapping resonances. Here one of the resonances may appear as some "background" onto which a neighboring resonance is superposed [28].

In Refs. [10, 26], the phase rigidity $|\rho|^2$ with

$$\rho = \frac{\int dr\ \hat{\Psi}(r)^2}{\int dr\ |\hat{\Psi}(r)|^2} = e^{2i\theta}\frac{\int dr\ ([{\rm Re}\hat{\Psi}(r)]^2 - [{\rm Im}\hat{\Psi}(r)]^2)}{\int dr\ ([{\rm Re}\hat{\Psi}(r)]^2 + [{\rm Im}\hat{\Psi}(r)]^2)} \tag{6}$$

defined at the energy $E$, is introduced in order to describe phenomenologically the influence of some impurity onto the phase of the scattering wave function $\hat{\Psi}_C^E$. We use this expression in order to get information on the phases of the $\hat{\Psi}_C^E$ in the regime of resonance overlapping.

The amplitude of the transmission through a quantum dot is [7]

$$t = -2\pi i \sum_\lambda \frac{\langle \xi_L^E | V | \phi_\lambda \rangle \langle \phi_\lambda^* | V | \xi_R^E \rangle}{E - z_\lambda}\,. \tag{7}$$

The eigenvalues $z_\lambda$ and eigenfunctions $\phi_\lambda$ of $H_{\rm eff}$ are involved in (7) with their full energy dependence [3]. According to (7), the transmission is resonant in relation to the real part of the eigenvalues of $H_{\rm eff}$. The transmission amplitude (7) can be rewritten by means of the scattering wave function (5),

$$t = -2\pi i\ \langle \xi_C^E | V | \hat{\Psi}_C^E \rangle \tag{8}$$

with $\hat{\Psi}_R^E$ being complex, in general. The advantage of this representation consists in the fact that it does not suggest the existence of Breit-Wigner peaks in the transmission probability. Quite the contrary, the transmission is determined by the degree of alignment of the wave function $\hat{\Psi}_C^E$ with the propagating modes $\xi_C^E$ in the leads, i.e. by the value $\langle \xi_C^E | V | \hat{\Psi}_C^E \rangle$. This alignment is important in the regime of overlapping resonances where the identification of single resonances and resonance states ceases to be meaningful. The expressions(7) and (8) are fully equivalent.

### C. Correlation measures

The redistribution processes taking place inside the system under the influence of the coupling to the continuum can be characterized by the number $N_\lambda^p$ of principal components of the eigenfunctions $\phi_\lambda$. Using (3) this number reads [29]

$$N_\lambda^p = \frac{1}{M \sum_{\lambda'=1}^{M} |b_{\lambda\lambda'}|^4} \quad ; \qquad |b_{\lambda\lambda'}|^2 = \frac{|d_{\lambda\lambda'}|^2}{\sum_{\lambda"=1}^{M} |d_{\lambda'\lambda"}|^2} \; . \tag{9}$$

In the limit of equal mixing of the state $\lambda$ with all states $\lambda'$, one gets $b_{\lambda\lambda'} = 1/\sqrt{M}$ for all $\lambda'$ and $N_\lambda^p = 1$. In the opposite case, we have $b_{\lambda\lambda'} = \delta_{\lambda,\lambda'}$ and $N_\lambda^p = 1/M$. In the first case the collectivity of the state $\lambda$ is large [4, 29]. Almost all components of the wave function have the same sign because the wave function of the state $\lambda$ is aligned to the scattering wave function $\xi_C^E$ of the channel $C$ at the cost of the other resonance states trapped by it. In the second case the wave functions $\lambda$ are not at all aligned to the $\xi_C^E$, and the signs of their different components are not the same. For details of the phenomenon of alignment see Ref. [5]. Generally, $1/M \leq N_\lambda^p \leq 1$.

Due to (5), the properties of the scattering wave function $\hat{\Psi}_C^E$ are determined by the properties of all the wave functions $\phi_\lambda$. Using the representation (3), we can write $\hat{\Psi}_C^E = \sum_\lambda \langle \phi_\lambda^B | \hat{\Psi}_C^E \rangle \; \phi_\lambda^B$ and define

$$N_E = \frac{1}{\sum_{\lambda=1}^{M} |\langle \phi_\lambda^B | \hat{\Psi}_C^E \rangle|^4} \; . \tag{10}$$

The normalization has to be done separately at every energy $E$ and coupling strength $v$. The value $N_E$ is a certain analogon to (9), but for the representation of the scattering wave function $\hat{\Psi}_C^E$ in the set of eigenfunctions $\phi_\lambda^B$ of the Hamilton operator $H_B$. Usually, $N_E$ is called inverse participation ratio. Further, we define the analogous expression

$$N_x = \frac{1}{|\langle \overline{x} | \hat{\Psi}_C^E \rangle|^4} \tag{11}$$

with $\hat{\Psi}_C^E = \langle \overline{x} | \hat{\Psi}_C^E \rangle \; \phi_\lambda^B$.

Another measure for coherence is the autocorrelation function of the fluctuation $\delta\sigma = \sigma - \overline{\sigma}$ of the cross section $\sigma$,

$$C(\varepsilon) = \frac{1}{\overline{\sigma}^2 |I|} \int_I \delta\sigma(E+\varepsilon)\delta\sigma(E) dE \; . \tag{12}$$

Here, $I$ is the same energy interval used to determine $\overline{\sigma}$ and $\delta\sigma = \sigma - \overline{\sigma}$. The Lorentzian shape of $C(\varepsilon)$ for small $\varepsilon$ is characteristic of Ericson fluctuations [13]. In the overlapping

regime, the width of the Lorentzian is large compared to the average spacing of the resonance states. Such a result has been found in many experimental data, above all in the analysis of nuclear reaction cross sections, e.g. [14]. It has been found recently also in high-resolution experimental data on the photoionization of atoms [15]. In the present paper, we will analyse the fluctuation picture of the transmission and denote the corresponding autocorrelation function by $C_G(\varepsilon)$.

## III. NUMERICAL RESULTS: TRANSMISSION THROUGH QUANTUM BILLIARDS, ENERGY-AVERAGED PHASE RIGIDITY AND COLLECTIVITY

The numerical calculations are performed for chaotic quantum billiards of different type in the tight-binding lattice model, for details see Datta [8] and [7]. The phase rigidity $\rho$ is calculated in the representation (6). The coupling strength $v$ between cavity and attached leads is the same for both leads. It is varied by means of $v \equiv \kappa/\kappa_0$ where $\kappa_0 = 1$ is the hopping matrix element inside the cavity as well as inside the lead while $\kappa$ is the hopping matrix element between cavity and lead. The cavities are small and the number of channels is one in each of the two attached identical leads. We trace transmission and phase rigidity (averaged over the whole energy window between 11 and 34, in units of the widths of the leads) as a function of the coupling strength $v$ between cavity and attached leads.

In Fig. 1, we present the numerical results for the transmission (top) through a Sinai billiard and for the phase rigidity (bottom) as a function of energy $E$ and coupling strength $v$. The shape of the billiard is shown in Figs. 5(a,b). Around $v \approx 1$, the transmission is enhanced and the phase rigidity is reduced at all energies. Analogous results (Fig. 2) are obtained for the transmission through a Sinai billiard with another geometry [Figs. 5(c,d)]. Comparing the two figures 1 and 2, we see that the transmission spectrum as well as the phase rigidity do change only a little when the geometry of the cavity is varied. This result coincides qualitatively with the high reproducibility of the experimental data observed in the fluctuations of the spectrum of the atom $^{85}Rb$ in strong crossed magnetic and electric fields [15].

In Fig. 3, we show the numerical results for the transmission through a billiard of Bunimovich type and the phase rigidity as a function of energy and coupling strength. In the calculations, the leads are attached in such a manner, see Figs. 5(e,f), that the

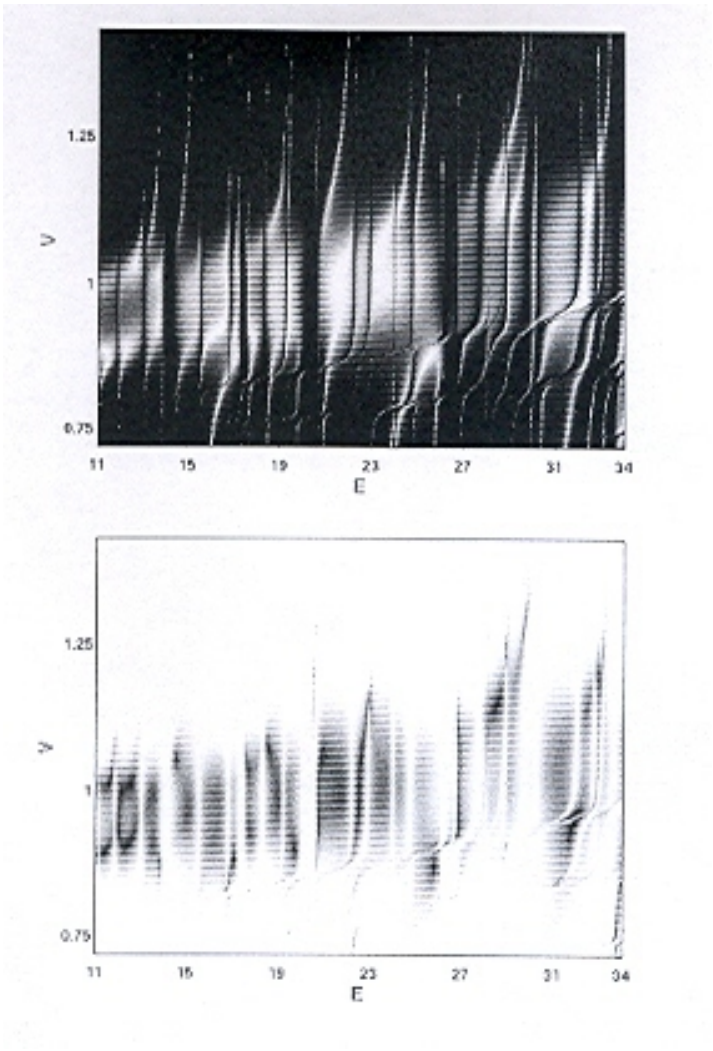



FIG. 1: Conductance $G = |t|^2$ (top) and phase rigidity $|\rho|^2$ (bottom) for a Sinai billiard as a function of energy $E$ and coupling strength $v$ between billiard and attached leads [30]. The transmission and the phase rigidity vary between 1 (white) and 0 (black). The shape of the billiard is shown in Figs. 5(a,b): size $x = 3,\ y = 7$, radius $R = 1.5$, in units of the width of the leads. The calculations are performed in the tight-binding lattice model [8].

transmission via short-lived whispering gallery modes is supported by the geometry of the billiard in the regime of overlapping resonances. The whispering gallery modes are especially stable as has been shown in earlier studies [31] and as it can be seen directly by comparing Figs. 1 and 2 with 3.

The correlation between the conductance $\langle G\rangle = \langle |t|^2\rangle$ and $1 - \langle |\rho|^2\rangle$ can be seen more directly from Fig. 4, where $\langle G\rangle$ and $\langle |\rho|^2\rangle$, averaged over energy, are shown as a function of

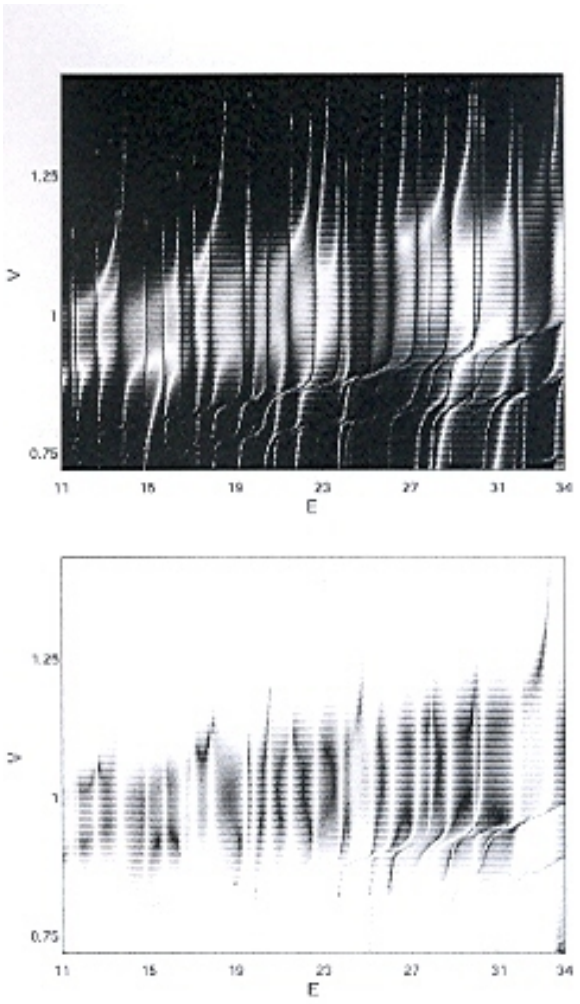



FIG. 2: The same as Fig. 1 but $x = 4, y = 5$. The shape of the billiard is shown in Figs. 5(c,d).

$v$ for the three cavities whose geometries are shown in Figs. 5(a–f). In all cases, $\langle G \rangle$ and $1 - \langle |\rho|^2 \rangle$ are strongly correlated. Around $v = 1$ $\langle G \rangle$ and $1 - \langle |\rho|^2 \rangle$ are maximum. Here also $N_E$, defined in (10), is maximum. When the parameters of the Sinai billiard are changed from $x = 3, y = 7$, Fig. 4(a), to $x = 4, y = 5$, Fig. 4(b), $\langle G \rangle$ and $\langle |\rho|^2 \rangle$ do change only a little.

The situation is however another one for transmission through a Bunimovich cavity in the regime of overlapping resonances. When the leads are attached in such a manner that the transmission via whispering gallery modes is supported then the transmission is more enhanced and the phase rigidity is more reduced [Fig. 4(c)] than in the case of the two Sinai billiards considered above. When the leads are attached in another manner to the

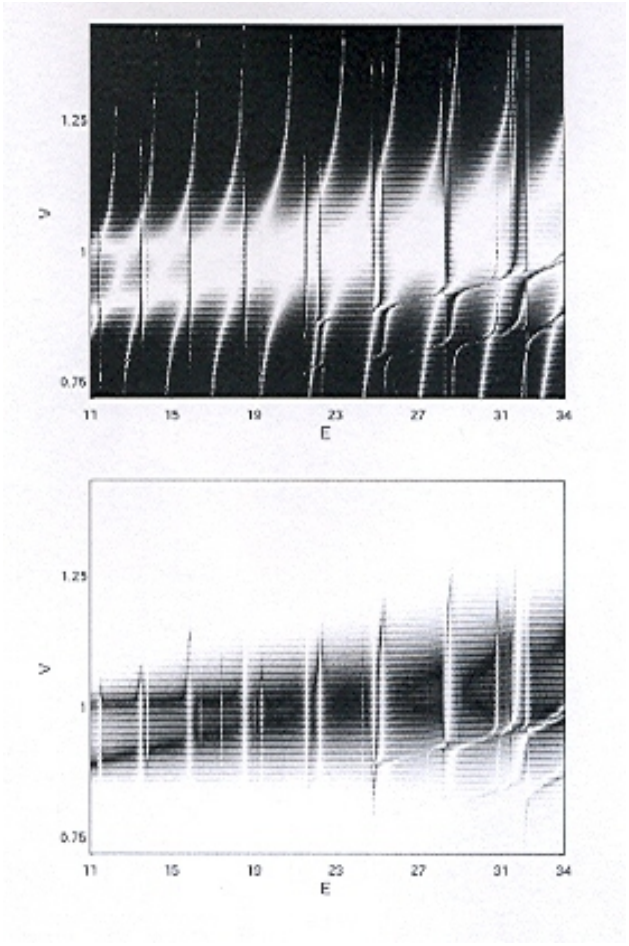



FIG. 3: The same as Fig. 1 but for a billiard of Bunimovich type to which the leads are attached in such a manner that transmission via whispering gallery modes is supported. The shape of the billiard is shown in Figs. 5(e,f): Radius $R = 3$ and distance $D = 2$ between the centers, in units of the width of the leads.

Bunimovich cavity so that they do not support transmission through whispering gallery modes, the transmission (averaged over energy) may be very small and, correspondingly, the phase rigidity (averaged over energy) remains large. For the geometry shown in Figs. 5(g,h), it is $\langle G \rangle \leq 0.1$ and $\langle |\rho|^2 \rangle \geq 0.9$. In this case, the whispering gallery modes are related, above all, to the reflection.

In Fig. 5, we show the wave functions $\phi_\lambda$ of a few short-lived and long-lived states in the four cavities considered. The corresponding eigenvalues $z_\lambda$ calculated at the energy $E$ are given in Table I. Although the wave functions are delocalized in space in all cases in the corresponding closed system, the short-lived states might be localized as can be seen from

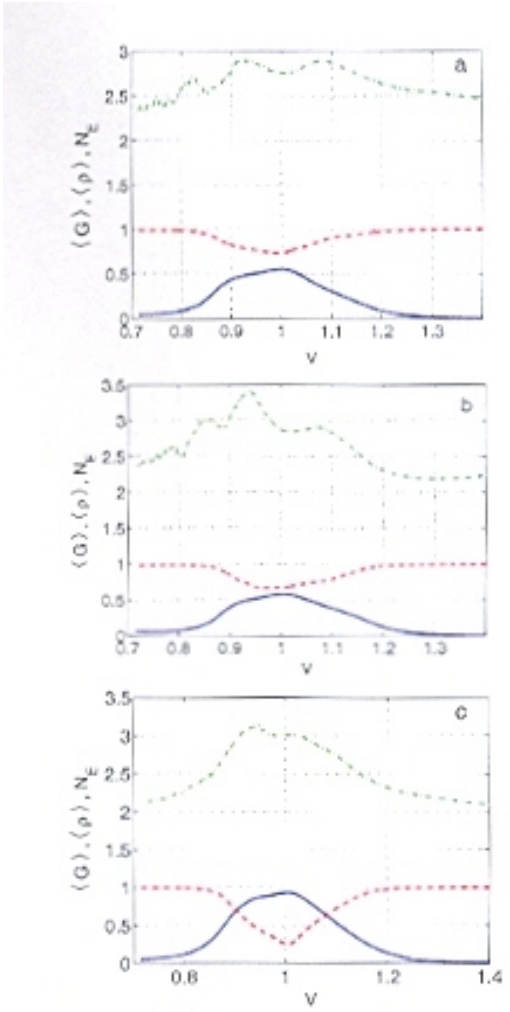



FIG. 4: (color online) Conductance $\langle G\rangle = \langle |t|^2\rangle$ (blue full line), energy-averaged phase rigidity $\langle |\rho|^2\rangle$ (red dashed line) and inverse participation ratio $N_E$ of the scattering wave function $\Psi_C^E$ (green dash-dotted line), averaged over the whole energy window ($11 \leq E \leq 34$), as a function of the coupling strength $v$, [30]. (a) Sinai billiard with $x = 3, y = 7, R = 1.5$ in units of the width of the leads [Figs. 5(a,b)]; (b) the same as (a) but $x = 4, y = 5$ [Figs. 5(c,d)]; (c) Bunimovich billiard with transmission through whispering gallery modes, $R = 3, D = 2$ in units of the width of the leads [Figs. 5(e,f)]. The calculations are performed in the tight-binding lattice model [8].

Figs. 5(a), (c), (e) and (g). Only the long-lived resonance states are delocalized inside the cavity, see Figs. 5(b), (d), (f) and (h).

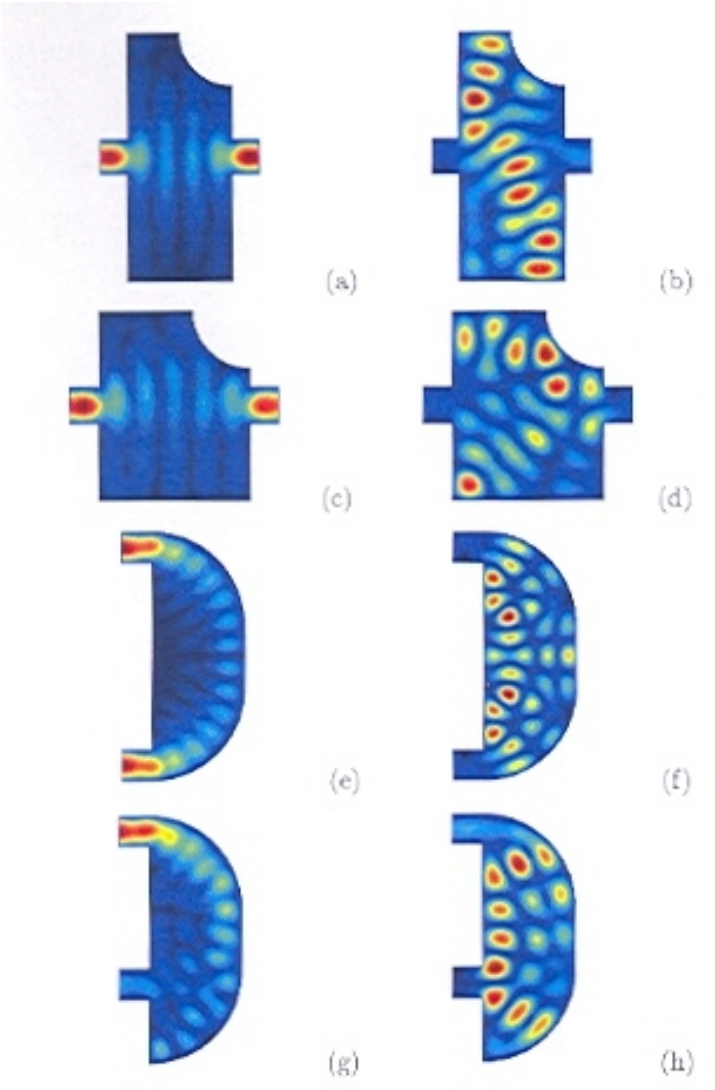



FIG. 5: (color online) Wave functions $\phi_\lambda$ of some short-lived and long-lived resonance states in the Sinai billiard (a,b) with $x = 3, y = 7$; (c,d) with $x = 4, y = 5$, and in the Bunimovich billiard (e,f) with leads attached for support of transmission via whispering gallery modes and (g,h) without support of whispering gallery modes. The corresponding eigenvalues $z_\lambda$ are given in Table I. The short-lived states (a,c,e,g) are localized in space and de-localized in energy while the long-lived states (b,d,f,h) are de-localized in space and localized in energy.

TABLE I: The eigenvalues $z_\lambda$ corresponding to the eigenfunctions $\phi_\lambda$ shown in Fig. 5, calculated at the energy $E$ and coupling strength $v = 1$.

| Figure | E | $z_\lambda$ |
|---|---|---|
| 5.a | 25 | $20.1228 - 3.1657\ i$ |
| 5.c | 25 | $18.4570 - 2.3354\ i$ |
| 5.e | 25 | $24.8227 - 2.4076\ i$ |
| 5.g | 20 | $22.7141 - 1.1801\ i$ |
| 5.b | 25 | $20.6891 - 0.0617\ i$ |
| 5.d | 25 | $22.6227 - 0.0635\ i$ |
| 5.f | 25 | $32.2046 - 0.0276\ i$ |
| 5.h | 20 | $18.3281 - 0.0713\ i$ |

## IV. PHASE RIGIDITY AND RESONANCE TRAPPING IN THE TRANSMISSION THROUGH FEW-SITES STRUCTURES

The results shown in Fig. 4 show some collective features involved in the scattering wave function $\Psi_C^E$. In order to understand these features better, we provide numerical results for simple structures with a small number of sites. First, we consider the one-dimensional case (chain) described by the tight-binding Hamilton operator

$$H = -\sum t_j |j\rangle\langle j+1| + c.c. \tag{13}$$

where $j$ runs over all sites of the system, i.e. over those of the left and right leads as well as over those of the one-dimensional box consisting of $N$ sites. The $t_j$ are the hopping matrix elements. Details of the model are given in [7]. The box is opened by varying the hopping matrix elements between leads and box in the following manner. We define $t_j = v_L$ if $j = j_{\rm in} - 1$; $t_j = v_R$ if $j = j_{\rm out}$; $t_j = 1$ in the leads and $t_j = t_0$ otherwise. In the case $t_0 = 1$, the eigenvalue spectrum $E_n = -2\,t_0\,cos(\frac{n\pi}{N+1})$ of $H_B$ is distributed over almost the whole propagation band $E(k) = -2\,cos(k)$. Our calculations are performed for symmetrical cases with $v_L = v_R \equiv v$. The phase rigidity is calculated from (6).

In Fig. 6, we show results of calculations obtained for a chain of length $M = 10$ with $t_0 = 1$. In the sub-figure 6(a,b) the conductance $G = |t|^2$ and the phase rigidity $|\rho|^2$ are

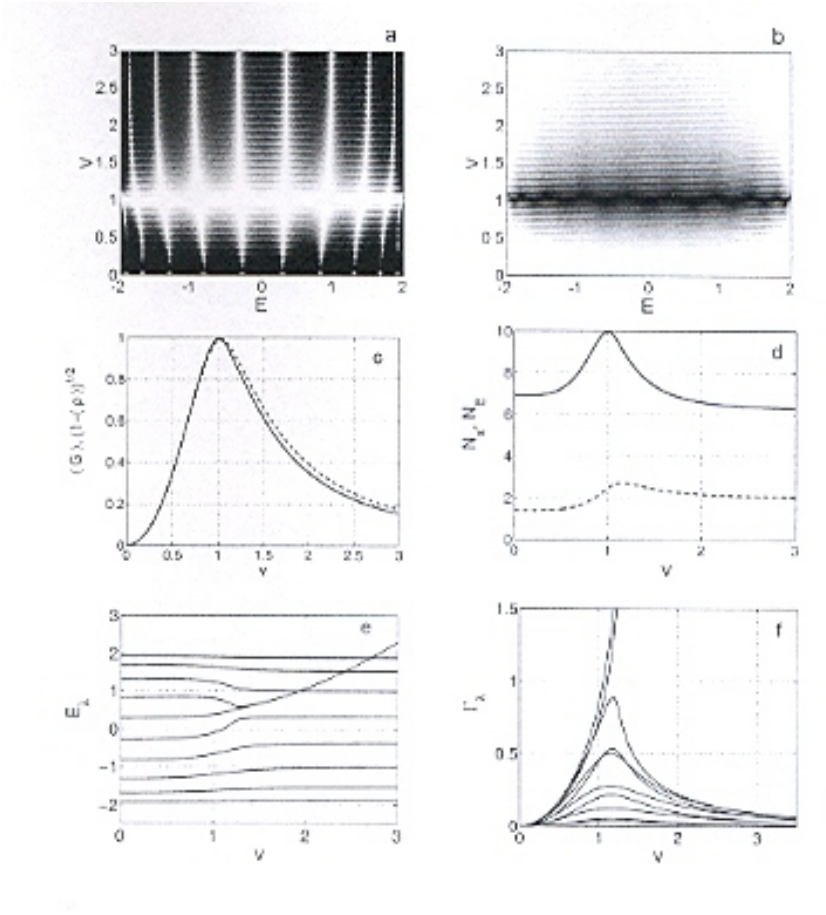



FIG. 6: (a): The conductance $G = |t|^2$ of a one-dimensional 10-sites chain, $t_0 = 1$, with wires attached at the ends of the chain ($j_{\rm in} = 1$, $j_{\rm out} = 10$) as a function of energy $E$ and coupling strength $v$ between the chain and the two wires [30]. The positions of the long-lived states at large coupling strength $v$ differ from the positions $E_\lambda^B$ (denoted by white circles). (b): The phase rigidity $|\rho|^2$ for the same 10-sites chain. (c): Transmission $\langle G\rangle$ (full line) and $\sqrt{1-\langle|\rho|^2\rangle}$ (dotted line), and (d): $N_x$ (full line) and $N_E$ (dotted line), as a function of the coupling strength $v$ for the 10-sites chain. The values $\langle G\rangle$, $\langle|\rho|^2\rangle$, $N_x$ and $N_E$ are averaged over energy in the whole energy window $-2 \le E \le 2$. (e) $E_\lambda$ and (f) $\Gamma_\lambda$ as a function of the coupling strength $v$. The $E_\lambda$ and $\Gamma_\lambda$ are calculated at $E = 0.5$. All calculations are performed in the tight-binding model [7].

shown as a function of energy $E$ and coupling strength $v$. These figures are very similar to Fig. 3 for the transmission through a quantum billiard with convex boundary in which the transmission occurs mainly via whispering gallery modes. In the one-dimensional chain (Fig. 6), we see threshold effects at $E = -2$ and $E = 2$ where the widths of the resonance

states approach zero. These threshold effects are excluded in Fig. 3 where the energy range $13 \leq E \leq 34$ is considered and the thresholds are at about $E = 10$ and 40. We conclude therefore that the one-dimensional chain mimics the transmission through the Bunimovich cavity occurring, at $v = 1$, mainly via whispering gallery modes. The transmission has a plateau at $v_{\rm cr} \approx 1$. In the case of the Bunimovich cavity, dips appear due to the long-lived trapped resonance states. Also the phase rigidity $|\rho|^2$ of the chain [Fig. 6(b)] shows a behavior similar to that obtained for the Bunimovich cavity. In the case of the chain, the transmission occurs clearly via traveling modes.

For further discussion, we show additionally in Fig. 6 some characteristic values discussed in the foregoing sections. Also in the one-dimensional chain, we see the anti-correlation between conductance $G = |t|^2$ and energy-averaged phase rigidity $|\rho|^2$ [Fig. 6(c)] that is observed in the billiards of Sinai and Bunimovich type (Figs. 4). The values $G = |t|^2$ and $\sqrt{1 - |\rho|^2}$, averaged over energy, are almost the same for all values $v$. Furthermore, $N_E$ is enhanced in the critical region around $v \approx 1$ [Fig. 6(d)] in a similar manner as in Fig. 4 for the cavities. Additionally, we show $N_x$ as a function $v$. It is also enhanced in the critical region.

In the chain, $N_x$ is smaller at $v \gg 1$ than at $v \ll 1$ according to the fact that the wave functions of the long-lived states appearing at large $v$ are, as a rule, more chaotic than the original ones at small $v$ (see e.g. [32]), i.e. they are distributed in $x$ with more or less equal probability over the whole cavity in contrast to the original states at small $v$. As to $N_E$, it shows the opposite behavior, i.e. it is larger at $v \gg 1$ than at $v \ll 1$. The reason is that the short-lived states are strongly correlated, i.e. the number $N_\lambda^p$ of principal components defined in (9), is large for every short-lived state [3, 29]. Due to this fact, $N_E$ remains comparably large when short-lived states are formed.

In the lower part of Fig. 6, we show the energies $E_\lambda$ and widths $\Gamma_\lambda$ of the 10 resonance states as a function of the coupling strength $v$. We see the formation of two short-lived states in the critical region $v \approx 1$ according to the fact that two (identical) wires are attached. The widths of all states are maximal in the center of the energy window due to the condition $\Gamma_\lambda \to 0$ for all $\lambda$ in approaching the thresholds $E \to \pm 2$. The short-lived states arise therefore from the middle of the spectrum. Their contribution is shifted to energies out of the window $-2 \leq E \leq 2$ when $E \neq 0$, see Fig. 6(e) calculated at $E = 0.5$. We see therefore only 8 resonances in the transmission when $v > 1$. Collective effects are maximal around

the critical value $v_{\rm cr} = 1$ being somewhat smaller than the value $v = 1.2$ at which the widths bifurcate. At $v_{\rm cr}$, many resonance states are almost aligned with the propagating modes $\xi_C^E$ in the leads, while at $v = 1.2$ two resonance states are aligned at maximum.

In order to get a better understanding for the appearance of collective effects in the critical region around $v_{\rm cr}$ we show in Figs. 7 to 10 the results of calculations performed for structures being more complicated than a chain. We performed the calculations for different positions $j_{\rm in}$ and $j_{\rm out}$ at which the wires are attached, and for different numbers $M$ of resonance states. We choose $t_0 = 0.05$ (instead of $t_0 = 1$ in Fig. 6). Due to the small value of $t_0$, the resonance states lie in the narrow energy range $-0.1 \leq E \leq 0.1$, threshold effects are excluded and the eigenvalues $z_\lambda$ are almost independent of energy.

In the sub-figures (a) of Figs. 7 to 10, we show the transmission $G = |t|^2$ against coupling strength $v$ and energy $E$ for different one-dimensional systems. The areas with $0.98 \leq |t|^2 \leq 1$ are encircled by red full lines and those with $0 \leq |t|^2 \leq 0.02$ by white dashed lines. In these areas, the transmission at a fixed value $v$ shows a plateau of about 1 and 0, respectively. While the positions in energy of the plateaus $|t|^2 \approx 1$ depend on $v$, the energies of the plateaus $|t|^2 \approx 0$ do almost not vary with $v$. They are corridor-like and divide the resonances into different groups. The number of corridors is equal to $j_{\rm in} - 1$ corresponding to an arrangement of the $M$ resonances in $j_{\rm in}$ groups. In each group, plateaus $|t|^2 \approx 1$ appear in the critical region of $v$, while the resonances cause transmission peaks of Breit-Wigner shape at $v \ll v_{\rm cr}$ and $v \gg v_{\rm cr}$. The number of transmission peaks is equal to the number $M$ of resonance states when $v \ll v_{\rm cr}$, but $M-2$ when $v \gg v_{\rm cr}$ due to the fact that two channels are open with which two of the resonance states align eventually in the critical region.

In Figs. 7 to 9, the wires are attached symmetrically each to one of the internal sites, $j_{\rm out} = M - j_{\rm in} + 1,\ j_{\rm in} > 1$. In difference to the case represented in Fig. 6, the incoming wave is split into two parts: both parts move in different directions each to one of the borders of the chain where it will be reflected. Then the two parts interfere and give rise to a complicated transmission picture. As a consequence of the interferences, the transmission picture does almost not depend on the number of the sites ($M = 10$ in Figs. 7 and 8, but $M = 11$ in Fig. 9). More important than the total number of sites is the distance of the attached wires from the border of the chain. When the distance is an odd number ($M_{\rm in} = 2,\ M_{\rm out} = M - 1$ in Fig. 7) there is a zero transmission corridor around $E = 0$, while the transmission is maximal around this energy when the distance is an even number

($M_{\rm in} = 3,\ M_{\rm out} = M - 2$ in Figs. 8 and 9). The transmission picture shows more structures when the symmetry is violated (Fig. 10 for $M = 11$ with $M_{\rm in} = 2,\ M_{\rm out} = M - 2$).

The regions of extremely low conductance (less than 0.02, corresponding to transmission gaps) and enhanced transmission (more than 0.98, corresponding to perfect conductance bands), marked in Figs. 7 to 9 by white dashed lines and red solid lines, respectively, are extended over comparably large energy regions. A similar result ("transmission gaps and sharp resonant states") has been found in recent numerical calculations for the transport through a simple mesoscopic device [33]. We underline that both the transmission plateaus with maximal transmission and the corridors of transmission zeros are the result of redistribution, interference and alignment processes. They can not be described by isolated Breit-Wigner resonances or isolated bound states in the continuum.

The redistribution processes taking place in the critical region around $v_{\rm cr} = \sqrt{t_0}$ of the coupling strength $v$ can be traced by comparing the sub-figures (b) of Figs. 7 to 10 with the corresponding sub-figures (c). In the sub-figures (b), the coupling coefficients $|v(n)|$ of the $M$ discrete states [eigenstates of $H_B$, Eq. (1)] to the propagating modes $\xi_C^E$ are shown. They are different for the different positions $j_{\rm in}$ of attached wires and different numbers $M$ of resonance states. Due to the symmetries involved in the considered chains, differences appear between the cases with an even and an odd number $M$ of resonance states. In the first case [$M = 10$, Figs. 7 and 8], the coupling coefficients $v(n)$ ($1 \le n \le M$) of all $M$ states to the continuum of propagating modes are different from zero while there is at least one state with $v(n) = 0$ in the last case [$M = 11$, Figs. 9 and 10]. Nevertheless, the eigenvalue trajectories [sub-figures (c)] are similar for the different cases with different $M$. They show the typical resonance trapping behavior known from studies on many different systems, see Ref. [3]. In the regime of overlapping resonances and two channels, the redistribution of the spectroscopic properties of the system takes place due to the alignment of two resonance states each with one of the two propagating modes (input and output channels). The redistribution occurs hierarchically [23, 24]: a resonance state will be trapped by overlapping with a neighboring state when its width is somewhat smaller than that of the neighboring state. The widths of trapped states cease from increasing with increasing coupling strength $v$. Instead, they mostly decrease and the positions in energy of the trapped states do almost not change with further increasing $v$, for details see Ref. [3].

The formation of zero-transmission corridors is directly related to the existence of trapped

resonance states. They appear independently of the existence of states whose coupling strength $v(n)$ is zero. Between the corridors, the redistribution processes create plateaus with an enhanced transmission. These plateaus are related directly to the avoided level crossings appearing in the regime of overlapping resonances. Unlike the zero-transmission corridors, the positions of the plateaus with maximal transmission depend on the coupling strength $v$.

In the sub-figures (d), the energy-averaged transmission $\langle G \rangle = \langle |t|^2 \rangle$ and the phase rigidity $\langle |\rho|^2 \rangle$ of the total scattering wave function $\Psi_C^E$ are shown. Like in the calculations for the microwave cavities, the transmission is enhanced and the phase rigidity is reduced in the critical region where the spectroscopic redistribution takes place.

The calculations for two-dimensional systems are performed in an analogous manner as those for one-dimensional systems, for details see Ref. [7]. The results are similar to those obtained for the one-dimensional systems. The main difference between the two cases is that there are more possibilities to influence the transmission picture in the two-dimensional systems than in the one-dimensional systems. An example is shown in Fig. 11. It is interesting to see that the areas with enhanced transmission may be shifted and that the corridors with zero-transmission zeros may be relatively broad.

Summarizing the results shown in Figs. 6 to 11 for different toy models, we state the following. The enhancement of the transmission seen in realistic systems in the crossover from the weak-coupling to the strong-coupling regime (Sect. III) is caused by spectroscopic redistribution processes taking place in the system under the influence of the coupling to the continuum. These redistribution processes are correlated with a reduced value of the phase rigidity and may be traced back to the well-known resonance trapping phenomenon occuring in open quantum systems at high level density when the resonance states overlap.

## V. FLUCTUATION OF THE TRANSMISSION PROBABILITY

We performed an analysis of the transmission through the considered cavities by means of the autocorrelation function of the transmission fluctuations $\delta G = \delta |t|^2 = |t|^2 - \langle |t|^2 \rangle$, see Eq. (12). In the calculations, $I = 23$ is the energy interval used to determine $\langle |t|^2 \rangle$, i.e. $11 \leq E \leq 34$ as shown in Figs. 1, 2 and 3. The area of all three cavities is of the same order of magnitude. The number of states is about 35 in the considered energy region

$11 \leq E \leq 34$. The average spacing of the states is about 0.65. There is one channel in each of the two identical attached leads.

In Fig. 12, we show the autocorrelation function $C_G(\varepsilon)$ for the transmission through the three cavities (considered in Sect. III) in the regime of overlapping resonances with avoided level crossings where the transmission is enhanced and the phase rigidity is reduced. At small $\varepsilon$, we see the Lorentzian-like shape characteristic of Ericson fluctuations [13]. When $v = 1$, the width of the Lorentzian is larger than the average spacing. Comparing the function $C_G(\varepsilon)$ of the two Sinai billiards with that for the transmission through the Bunimovich cavity via whispering gallery modes we see that the width of the Lorentzian is larger for the Bunivovich billiard than that for the two Sinai billiards. In all three cases, the width becomes smaller with decreasing as well as with increasing coupling strength, $v = 0.9$ and 1.1, respectively. Enlarging $v$ further, we arrive in the regime of separated time scales. Here, $C_G(\varepsilon)$ falls off in a smaller region $\varepsilon$ than in the regime with overlapping resonances. That means, the correlation between the long-lived states is small at large $v$ and is comparably in value with the correlations between almost isolated resonance states (at small $v$).

As can be seen from Fig. 12, the function $C_G(\varepsilon)$ is still large at larger $\varepsilon$, especially in the case of the Bunimovich cavity. This result points to long-range correlations existing between the different states, above all between different short-lived states. The oscillations differ from one another in the three considered cases. Related to this statement, we point to another result of our calculations: in the autocorrelation function $C_G(\varepsilon)$ at $v \gg 1$, we have small "peaks" (instead of oscillations) that are related to distant narrow resonance states.

In Fig. 13, the autocorrelation function $C_G$ versus energy $E$ and coupling strength $v$ is shown for the transmission through the 11-sites chains, represented in the insets of the sub-figures (c) of Figs. 9 and 10 with, respectively, symmetrically and non-symmetrically attached leads, for four different values $v$ around the critical value $v_{\rm cr}$. Both cases show the Lorentzian-like peak with maximum in the critical region $v = v_{\rm cr} = \sqrt{t_0} \approx 0.2$. The width of the peak increases with $v$ as long as $v < v_{\rm cr}$. This result agrees with theory [13]. Approaching however $v_{\rm cr}$, the width of the Lorentzian is not well defined. For $v > v_{\rm cr}$, the mean width of the long-lived resonance states decreases as $v^{-2}$ (see e.g. Fig. 6), while the width of the Lorentzian decreases much less. The structure of the autocorrelation function is more pronounced in the non-symmetrical case than in the symmetrical one. Altogether, the results agree with those obtained for the Sinai and Bunimovich cavities (Fig. 12).

The fluctuations in the transmission picture result, of course, from interferences. However, the alignment of some of the wave functions with the propagating modes in the wires plays an important role. It is expressed by the phase rigidity as shown in Sects. III and IV. The numerical results on the fluctuations demonstrate the weak dependence of the structure of the transmission picture on external parameters such as the shape of the billiard in Sect. III or the number of sites in the chains in Sect. IV. They are a hint to the existence of collective effects, that are large in the regime of overlapping resonances.

We mention here the results of three completely different experimental studies that qualitatively agree with our theoretical results on the collective effects observed in the conductance in the regime of overlapping resonances. First, the directly measured average life time of compound nucleus states in $^{58,60}Ni(p,p')$ is significantly smaller than that of the observed structures in the excitation function. Moreover, it decreases with increasing bombarding energy of the projectile and is smaller than the average distance between the states [34]. Secondly, a surprisingly high reproducibility of the fluctuation picture has been observed in high-resolution experimental results on Ericson fluctuations in atoms [15]. Thirdly, long-range correlations between individual resonance states have been found experimentally in an open microwave billiard [11].

## VI. DISCUSSION OF THE RESULTS AND SUMMARY

In this paper, we studied the transmission through different mesoscopic systems with $M$ states as a function of the coupling strength $v$ between system and attached leads and wires, respectively. We considered the two-channel case, i.e. one propagating mode in each of the two attached identical leads (wires). The numerical calculations are performed by using the Green function method (without any statistical assumptions). The results show the following features. At small $v$, the transmission picture consists of $M$ isolated resonance peaks (corresponding to standing waves) while $M-2$ narrow resonances are superposed by a smooth "background" transmission (caused by the two traveling modes) at large $v$. Most interesting are the results in the regime of strongly overlapping resonance states where the crossover from standing to traveling waves takes place. Here, the transmission is enhanced.

According to our results, the crossover occurs by means of the alignment of the wave functions of the individual resonance states each with one of the propagating modes $\xi^E_{C=R}$

and $\xi^E_{C=L}$ in the two leads. The alignment of the resonance states occurs stepwise. It is accompanied, at each step, by a certain decoupling of at least one neighboring resonance state from the continuum of propagating modes *(resonance trapping)*. For the mathematical foundation of the alignment phenomenon in open quantum systems see Ref. [5].

Resonance trapping in the regime of overlapping resonance states occurs hierarchically as can be seen from Figs. 6 to 11. It is a collective effect to which, eventually, all the states in the considered energy region contribute. Therefore, also the reduction of the phase rigidity and the enhancement of observable values, such as the transmission, are collective effects in the considered energy region. The reduction of the phase rigidity and the enhancement of the transmission are maximal when a large number of individual resonance states is almost aligned with the propagating modes in the leads. This happens at a coupling strength $v$ being somewhat smaller than the critical one at which the number of aligned resonance states is exactly equal to the number of propagating modes (channels). This situation is illustrated best by the whispering gallery modes appearing in a cavity of Bunimovich type, Fig. 3, see also Figs. 6 to 11.

Most interesting result of our numerical studies is that, in the regime of overlapping resonances, the conductance $\langle G\rangle$ is enhanced and correlated with $1-\langle|\rho|^2\rangle$. For certain values of the coupling strength $v$ between system and environment, the conductance is plateau-like in some finite energy regions $\Delta E$. Furthermore, corridors with zero transmission (total reflection) may appear as a function of the coupling strength $v$ due to destructive interferences between neighboring resonance states. The transmission picture with plateaus of maximal transmission and corridors of zero transmission is only weakly influenced by the spectrum of the closed system. It results mainly from collective interference effects.

The relation of the results obtained by us to the idea of standing waves in almost closed systems and traveling waves in open systems [12] is the following. In an almost closed system it is $H_{\rm eff}\approx H_B$, while in a strongly opened system the main term of $H_{\rm eff}$ is the coupling term $\sum_{C=L,R}V_{BC}(E^+-H_C)^{-1}V_{CB}$ via the continuum, see Eq. (1). The first case is realized in the regime of non-overlapping resonances while in the second case a smooth background (arising from the short-lived resonances) is superimposed by long-lived narrow (non-overlapping) resonances. Furthermore, the monochromatic source considered in Ref. [12] corresponds to the one-channel continuum represented by the propagating modes in (1). It is therefore not astonishing that the results obtained from (7) for the transmission

amplitudes in the two borderline cases fit well to the picture described in Ref. [12] for waves propagating in a random medium. However, the crossover between the two borderline cases is described differently in the two methods. In [12] a simple interpolation between the two regimes is proposed. In our formulation, however, the crossover between the two regimes is calculated in a straightforward manner. The two equivalent exact expressions (7) and (8) are used for, respectively, the two limiting cases and the crossover regime with overlapping resonances. As a result of these calculations, we received the result that the crossover regime is dominated by coherent collective phenomena.

The collective effects in the regime of overlapping resonance states influence also the autocorrelation function of the fluctuations of the transmission probability. Long-range correlations do appear. The autocorrelation function does not depend sensitively on external parameters such as the shape of the Sinai billiard. The high reproducibility of the fluctuation picture observed experimentally on atoms [15] fits into this picture. Furthermore, our results coincide with those obtained in Ref. [16]: in the few-channel case, Ericson-like fluctuations are determined by collective coherent interferences between the resonance states.

Summarizing we state the following. The transition from the weak-coupling to the strong-coupling regime is controlled by a redistribution of the spectroscopic properties of the system under the influence of the environment to which the system is coupled (by attaching leads to it). The redistribution consists in the alignment of a few resonance states each with one of the propagating modes in the leads. The alignment is a collective effect to which all resonance states in the considered energy region contribute: it occurs hierarchically by trapping neighboring resonance states which are more weakly coupled to the continuum of propagating modes than those which align. Eventually, the number of aligned resonance states is equal to the number of propagating modes in the leads. Due to their short life time (large decay width), the aligned resonance states form the background scattering on which the trapped resonance states appear as narrow resonances. Since they are aligned with the propagating modes $\xi_C^E$ in the leads, these short-lived resonance states may be identified with traveling modes.

**Acknowledgments**

We thank the Max Planck Institute for the Physics of Complex Systems for hospitality.

---

[1] H. Feshbach, Ann. Phys. (N.Y.) **5**, 357 (1958); **19**, 287 (1962).

[2] S. Drozdz, J. Okołowicz, M. Płoscajczak, and I. Rotter, Phys. Rev. C **62**, 024313 (2000).

[3] I. Rotter, Rep. Prog. Phys. **54**, 635 (1991); J. Okołowicz, M. Płoszajczak, and I. Rotter, Phys. Rep. **374**, 271 (2003).

[4] G.L. Celardo, F.M. Izrailev, V.G. Zelevinsky, and G.P. Berman, Phys. Rev. E **76**, 031119 (2007).

[5] I. Rotter, J. Phys. A **40** (2007) [quant-ph 0708.3891 (2007)].

[6] N. Moiseyev, Phys. Rep. **302**, 211 (1998).

[7] A.F. Sadreev and I. Rotter, J. Phys. A **36**, 11413 (2003).

[8] S. Datta, *Electronic transport in mesoscopic systems*, Cambridge University Press, 1995.

[9] A. Pandey and M.L. Mehta, Commun. Math. Phys. **87**, 449 (1983).

[10] P.W. Brouwer, Phys. Rev. E **68**, 046205 (2003).

[11] Y.H. Kim, U. Kuhl, H.J. Stöckmann, and P.W. Brouwer, Phys. Rev. Lett. **94**, 036804 (2005).

[12] R. Pnini and B. Shapiro, Phys. Rev. E **54**, R1032 (1996).

[13] T. Ericson, Phys. Rev. Lett. **5**, 430 (1960); Ann. Phys. (N.Y.) **23**, 390 (1963), reprinted **281**, 494 (2000).

[14] P. von Brentano, J. Ernst, O. Häusser, T. Mayer-Kuckuk, A. Richter and W. von Witsch, Phys. Lett. **9**, 48 (1964); T. Ericson and T. Mayer-Kuckuk, Ann. Rev. Nucl. Sci. **16**, 183 (1966).

[15] G. Stania and H. Walther, Phys. Rev. Lett. **95**, 194101 (2005).

[16] E. Narevicius and N. Moiseyev, Phys. Rev. Lett. **84**, 1681 (2000); J. Chem. Phys. **113**, 6088 (2000).

[17] E. Persson, I. Rotter, H.J. Stöckmann, and M. Barth, Phys. Rev. Letters **85**, 2478 (2000); H.J. Stöckmann, E. Persson, Y.H. Kim, M. Barth, U. Kuhl, and I. Rotter, Phys. Rev. E **65**, 066211 (2002).

[18] S.Y. Kun, Phys. Rev. A **65**, 034701 (2002).

[19] I. Rotter and A.F. Sadreev, Phys. Rev. E **69**, 066201 (2004).

[20] I. Rotter and A.F. Sadreev, Phys. Rev. E **71**, 036227 (2005).

[21] E.N. Bulgakov, I. Rotter and A.F. Sadreev, Phys. Rev. E **74**, 056204 (2006).

[22] P. Kleinwächter and I. Rotter, Phys. Rev. C **32**, 1742 (1985).

[23] W. Iskra, I. Rotter, and F.M. Dittes, Phys. Rev. C **47**, 1086 (1993).

[24] M. Müller, F.M. Dittes, W. Iskra, and I. Rotter, Phys. Rev. E **52**, 5961 (1995).

[25] E. Persson, K. Pichugin, I. Rotter, and P. Seba, Phys. Rev. E **58**, 8001 (1998); P. Seba, I. Rotter, M. Müller, E. Persson, and K. Pichugin, Phys. Rev. E **61**, 66 (2000); I. Rotter, E. Persson, K. Pichugin, amd P. Seba, Phys. Rev. E **62**, 450 (2000).

[26] S.A. van Langen, P.W. Brouwer, and C.W.J. Beenakker, Phys. Rev. E **55**, 1 (1997).

[27] I. Rotter, Phys. Rev. E **68**, 016211 (2003).

[28] A.I. Magunov, I. Rotter and S.I. Strakhova, Phys. Rev. B **68**, 245305 (2003).

[29] C. Jung, M. Müller, and I. Rotter, Phys. Rev. E **60**, 114 (1999).

[30] The critical value $v_{\rm cr}$ of the coupling strength is determined by the ration $v/\kappa_0$ and $v/t_0$, respectively. In the figure, we show also results obtained numerically for $v > v_{\rm cr}$.

[31] R.G. Nazmitdinov, K.N. Pichugin, I. Rotter, and P. Šeba, Phys. Rev. E **64**, 056214 (2001); Phys. Rev. B **66**, 085322 (2002).

[32] F.M. Dittes, I. Rotter, and T.H. Seligman, Physics Letters A **158**, 14 (1991).

[33] H. Al-Wahsh, E.H. El Boudouti, B. Djafari-Rouhani, A. Akjouj, and L. Dobrzynski, Phys. Rev. B **75**, 125313 (2007).

[34] E.P. Kanter, D. Kollewe, K. Komaki, I. Leuca, G.M. Temmer, W.M. Gibson, Nucl. Phys. A **299**, 230 (1978).

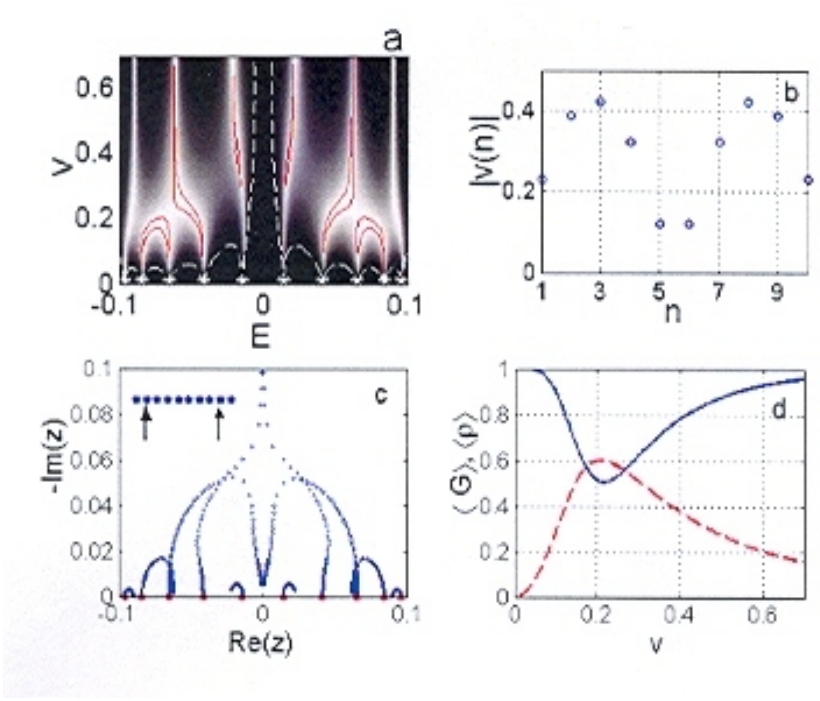



FIG. 7: (color online) The transmission through a one-dimensional chain of 10 sites, see the inset of sub-figure (c). The arrows show the sites at which the two (left and right) wires are attached. The hopping matrix elements inside the chain are 0.05 while those inside the attached wires are 1. (a) Conductance $G$ versus incident energy $E$ and coupling matrix element $v_L = v_R = v$, [30]. The white dashed lines show regions of extremely low conductance (less than 0.02, corresponding to transmission gaps) while the red solid lines show regions with enhanced transmission (more than 0.98, corresponding to perfect conductance bands). The positions of the bound states are shown by white stars. (b) The coupling matrix elements $|V_n| = |\psi_n(2)| = |\psi_n(9)|$ between the wires and the chain, $\psi_n(j)$, are the eigenfunctions of the "closed" chain described by $H_B$, see Eq. (1). (c) Evolution of the complex eigenvalues $z_\lambda$ of the effective Hamilton operator, Eq. (1), with increasing coupling strength $v$. The $z_k$ are calculated in site representation according to Datta [8]. The values at $v = 0$ are shown by red circles. (d) Evolution of the mean conductance $\langle G \rangle$ (red broken line) and energy-averaged phase rigidity $\langle |\rho|^2 \rangle$ (blue full line) with $v$. Note the hierarchical trapping of resonance states shown in (c): The resonance states 1 and 5 (10 and 6) are trapped already at small $v$. The state 3 (8) first traps the state 2 (9) and becomes trapped by the state 4 (7) at larger $v$. The two states 4 and 7 align with the two states in the two channels.

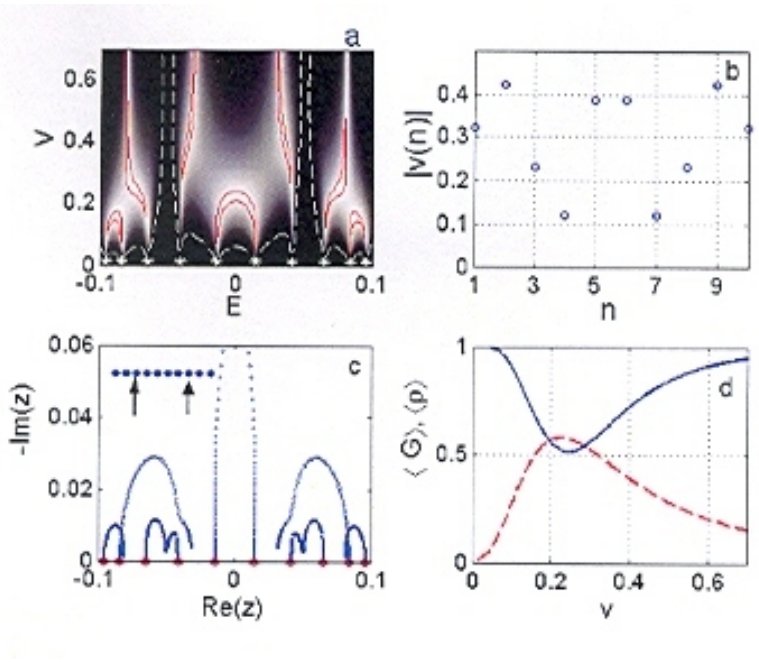



FIG. 8: (color online) The same as Fig. 7 but $|V_n| = |\psi_n(3)| = |\psi_n(8)|$ in (b). Note that resonance trapping shown in (c) starts at larger values of $v$ than in Fig. 7. Resonance state 2 (9) traps first the resonance states 1, 3, 4 (10, 8, 7) and becomes trapped by state 5 (6) at larger $v$. The two states 5 and 6 in the center of the spectrum align with the two states in the two channels.

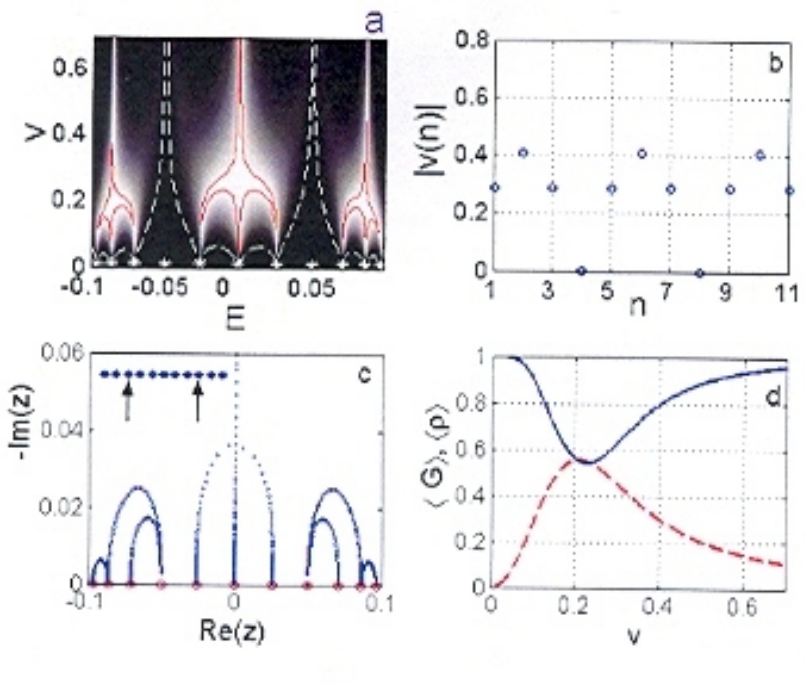



FIG. 9: (color online) The same as Fig. 7 but for a chain of 11 sites and $|V(n)| = |\psi_n(3)| = |\psi_n(9|$ in (b). Note that $|\mathrm{Im}(z_\lambda)|$ of the resonance state 4 (8) does not increase with increasing $v$ even at small $v$, i.e. this state is trapped already at very small $v$. The state 5 (or 7) traps first the states 1, 2, 3 (11, 10, 9) and becomes trapped by the state 6 (in the center of the spectrum) at larger $v$. Finally, also in this case $|\mathrm{Im}(z_\lambda)|$ of 2 states is large at large $v$, i.e. two states are aligned each to one of the states in the two leads.

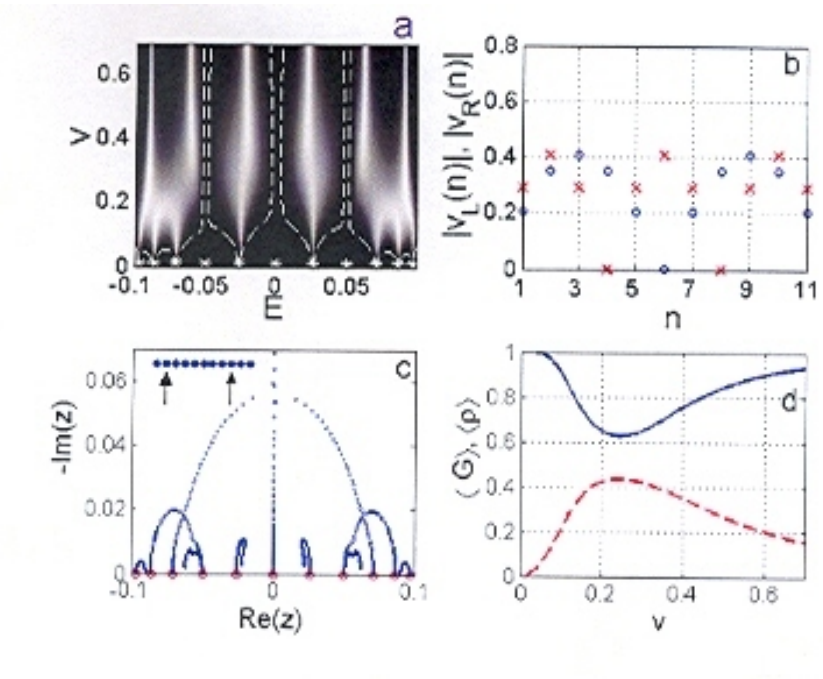



FIG. 10: (color online) The same as Fig. 7 but for a chain of 11 sites and $|V_L(n)| = |\psi_n(2)|$ (blue circles), $|V_R(n)| = |\psi_n(9)|$ (red crosses) in (b). The regions with enhanced transmission (more than 0.98, corresponding to perfect conductance bands) are small and not shown. Note the hierarchical resonance trapping also in this case. The resonance states 1, 4, 5 (11, 8, 7) are trapped at relatively small $v$ while the state 2 (10) first traps the neighboring states and then becomes trapped by the state 3 (9) at larger $v$. With further increasing $v$, the state 3 (9) becomes trapped by the state 6 in the center of the spectrum. Finally, there are two states (6 and 3 or 9) with large widths the wave functions of which are aligned each to one of the two wave functions in the two leads.

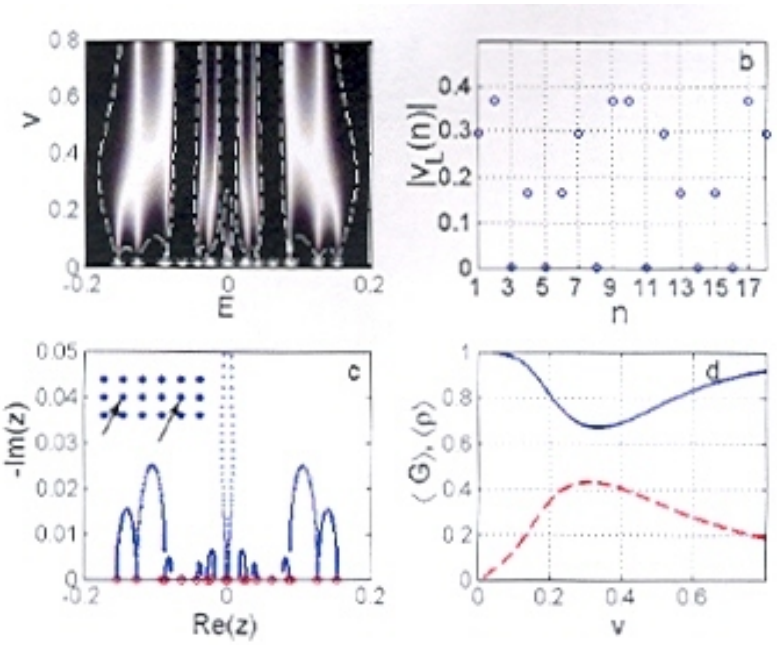



FIG. 11: (color online) The same as Fig. 7 but for a rectangle of 6 sites along the x-direction and 3 sites along the y-direction, see the inset in (c). The coupling matrix elements $|V_L(m,n)| = |\psi_{m,n}(i=2,j=2)|$, $|V_R(m,n)| = |\psi_{m,n}(i=5,j=2)|$ coincide because of the symmetry of the system, the $\psi_{m,n}(i,j)$ are the eigenfunctions of the "closed" rectangle described by $H_B$, see Eq. (1). The regions with enhanced transmission (more than 0.98, corresponding to perfect conductance bands) are small and not shown. Note that $|\mathrm{Im}(z_\lambda)|$ of the resonance state 4 (10) does not increase with $v$ even at very small $v$. Resonance trapping occurs hierarchically first around the center of the spectrum and then at its edges. Finally, two resonance states align to the two scattering states in the two leads.

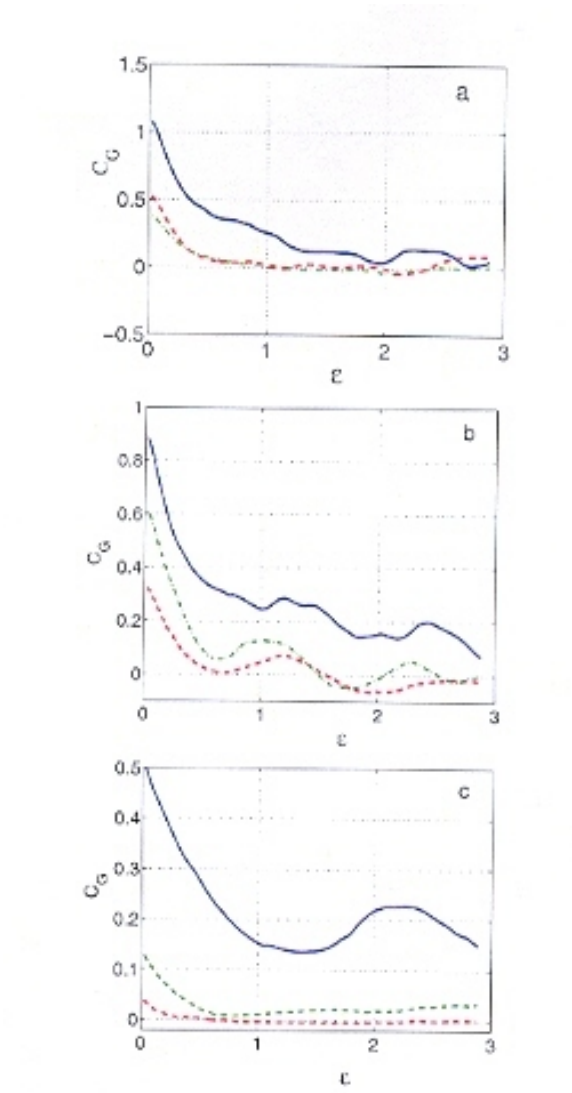



FIG. 12: (color online) The autocorrelation function $C_G(\varepsilon)$ for the transmission through the Sinai billiard with $x = 3, y = 7$ (a), with $x = 4, y = 5$ (b) and through the Bunimovich billiard via whispering gallery modes (c). In all three cases, the autocorrelation function is calculated for the whole energy window $11 \leq E \leq 34$ and shown for $v = 0.9$ (red dashed line), $v = 1$ (blue full line) and $v = 1.1$ (green dash-dotted line).

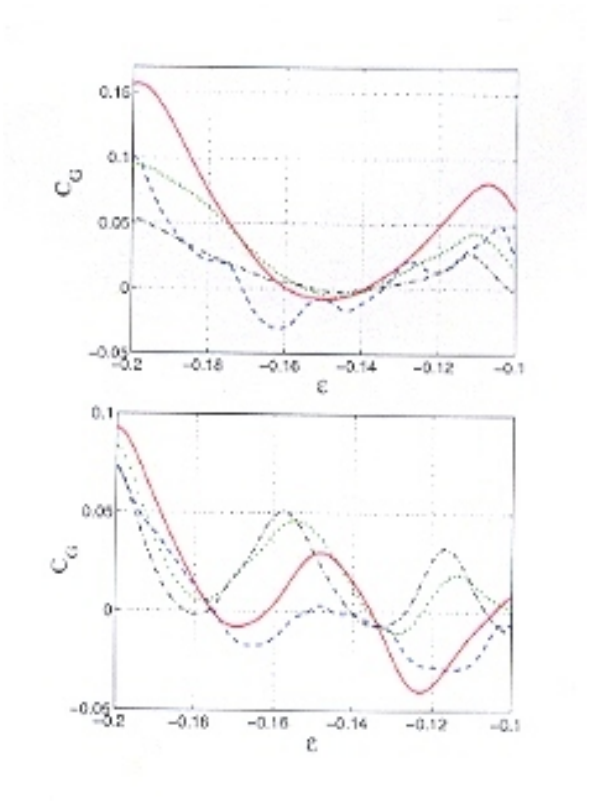



FIG. 13: (color online) The autocorrelation function $C_G(\varepsilon)$ for the conductance $G = |t|^2$ of the 11-sites chain with, respectively, symmetrically (top) and non-symmetrically (bottom) attached leads [see the insets of the sub-figures (c) of Figs. 9 and 10] for four different values of the coupling strength $v$: $v = v_{\rm cr} - 0.1$ (dashed blue curves), $v = v_{\rm cr}$ (solid red curves), $v = v_{\rm cr} + 0.1$ (dotted green curves), and $v = v_{\rm cr} + 0.2$ (dash-dotted black curves).